The Remarkable Structure and Dynamics of Tris(allyl)rhodium and -iridium as Determined by Theory and Experiment

Kevin D. John,*,† Ryszard Michalczyk,‡ Griselda Hernandez,‡ Jennifer C. Green,§ Richard L. Martin,⊥ R. Thomas Baker,† and Alfred P. Sattelberger†

Los Alamos Catalysis Initiative, Chemistry Division, MS J514, Los Alamos National Laboratory, Los Alamos, New Mexico 87545, Bioscience Division, B-3, MS G758, Los Alamos National Laboratory, Los Alamos, New Mexico 87545, Inorganic Chemistry Laboratory, University of Oxford, South Parks Road, Oxford OX1 3QR UK, and Theoretical Division, T-12, MS B268, Los Alamos National Laboratory, Los Alamos, NM 87545

Received August 5, 2002

The molecular geometries and electronic structures of M(η^3-allyl)$_3$ [M = Rh, Ir] have been calculated by both hybrid and gradient-corrected density functional theory (DFT). Hybrid DFT (B3LYP) calculations predict a global minimum of C_1 symmetry for both species. For Ir(allyl)$_3$ a local minimum of C_{3h} symmetry was also located ca. 3 kcal/mol above the C_1 ground state. These two minima are related by a σ-allyl transition state with a barrier of ca. 21 kcal/mol. The C_1 symmetry global minimum contains two basal allyls and an apical allyl ligand that can rotate about its axis through a concerted motion involving two distinct transition states of C_s symmetry (activation energy $\Delta E^{\ddagger} \cong 10$ kcal/mol). Variable-temperature ^{13}C NMR analysis of the Ir analogue confirms the C_1 ground state and validates the predicted activation energy experimentally (9.9 ± 1.4 kcal/mol). Additional evidence for the C_1 ground state comes from the good agreement of the calculated B3LYP Raman spectrum with experiment. Dynamic ^{1}H and ^{13}C NMR spectra of Rh(allyl)$_3$ provide evidence for three different fluxional processes, corresponding to the three transition states discussed above. Finally, the electronic structure of both complexes has been studied both experimentally and theoretically using photoelectron spectroscopy (PES) and gradient-corrected DFT calculations using the C_1 symmetry geometry obtained from hybrid DFT methods.

Introduction

Despite the large number of studies of compounds possessing allyl metal fragments,[1] little is known about the fundamental structure and reactivity of homoleptic transition metal allyl complexes. We are particularly interested in M(allyl)$_3$ [M = Cr, Rh, Ir][2] complexes due in part to their volatility and reactivity with solid supports that make them useful as CVD materials and catalyst precursors, respectively.

The reactivity of Cr(allyl)$_3$ and Rh(allyl)$_3$ with metal-oxide supports has been studied extensively.[3] In particular, moieties derived from Cr(allyl)$_3$ bound to highly dehydroxylated silica are active catalysts for olefin polymerization. In addition to surface reactivity, Rh(allyl)$_3$ has also been the subject of several solution reactivity studies mainly focused on protonolysis.[2] We have recently expanded the scope of both the Rh(allyl)$_3$ and Ir congener solution reactivity through studies involving a variety of C, S, and P donor ligands.[4] In the case of Co(allyl)$_3$ there has been only one report in the literature due to the fact that this complex is not very stable above −70 °C.[5]

Although the M(allyl)$_3$ class of molecules has been the subject of several reactivity studies, none of these complexes have been structurally characterized.[6] Attempts within our group to structurally characterize both Rh(allyl)$_3$ and Ir(allyl)$_3$ using single-crystal X-ray diffraction methods have so far been unsuccessful.[7]

† Los Alamos Catalysis Initiative, Los Alamos National Laboratory.
‡ Bioscience Division, Los Alamos National Laboratory.
§ University of Oxford.
⊥ Theoretical Division, Los Alamos National Laboratory.

(1) Sweany, R. L. [Co]; Sharp, P. R. [Rh]; Atwood, J. D. [Ir] In *Comprehensive Organometallic Chemistry*; Wilkinson, G., Stone, F. G. A., Abel, E. W., Eds.; Pergamon: Oxford, 1982; Chapter 5, pp 1, 115, 303. (b) Kemmitt, R. D. W.; Russell, D. R. [Co]; Hughes, R. P. [Rh]; Leigh, G. J.; Richards, R. L. [Ir] In *Comprehensive Organometallic Chemistry II*; Abel, E. W., Stone, F. G. A., Wilkinson, G., Eds.; Pergamon: Oxford, 1995; Chapter 5, pp 1, 277, 541. (c) White, C. *The Organometallic Chemistry of Cobalt, Rhodium, and Iridium*; Chapman and Hall: New York, 1985.

(2) O'Brien, S.; Fishwick, M.; McDermott, B.; Wallbridge, M. G. H.; Wright, G. A. *Inorg. Synth.* **1972**, *13*, 73. [Rh] Powell, J.; Shaw, B. L. *J. Chem. Soc. (A)* **1968**, 583. [Ir] Chini, P.; Martinengo, S. *Inorg. Chem.* **1967**, *6*, 837.

(3) Bade, O. M.; Blom, R.; Ystenes, M. *Organometallics* **1998**, *17*, 2524, and references therein. [Rh] (a) Basset, J. M.; Lefebvre, F.; Santini, C. *Coord. Chem. Rev.* **1998**, *178−180*, 1703. (b) Chang, T.; Bernasek, S. L.; Schwartz *Langmuir* **1991**, *7*, 1413. (c) Foley, H. C.; DeCanio, S. J.; Tau, K. D.; Chao, K. J.; Onuferko, J. H.; Dybowski, C.; Gates, B. C. *J. Am. Chem. Soc.* **1983**, *105*, 3074.

(4) John, K. D.; Salazar, K. V.; Scott, B. L.; Baker, R. T.; Sattelberger, A. P. *Chem. Commun.* **2000**, 581. (b) John, K. D.; Salazar, K. V.; Scott, B. L.; Baker, R. T.; Sattelberger, A. P. *Organometallics* **2001**, *20*, 296.

(5) Bönnemann, H.; Grard, C.; Kopp, W.; Pump, W.; Tanaka, K.; Wilke, G. *Angew. Chem., Int. Ed. Engl.* **1973**, *12*, 964.

(6) There is a footnote on page 966 of ref 5 that states that an X-ray structure analysis on Rh(allyl)$_3$ provided a C_s-a solution, but that satisfactory refinement was not possible due to "decomposition of the sample in the X-ray beam".

10.1021/om020632p CCC: $22.00
Publication on Web 11/15/2002

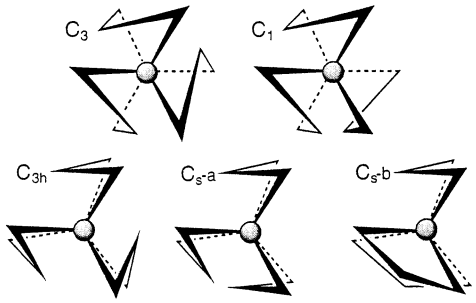

Figure 1. Possible geometries of the octahedral and trigonal prismatic forms of M(allyl)$_3$.

However, the structures of some of these complexes have been inferred on the basis of experimental evidence (NMR, PES) and theoretical methods. The electronic structure of Cr(allyl)$_3$ was investigated using PES techniques,[8] and the ground state structure was proposed to be of C_{3h} symmetry (trigonal prismatic, Figure 1) on the basis of Hartree−Fock and DFT calculations.[9] In the case of Co(allyl)$_3$, a C_s symmetry ground state structure (C_s-a, Figure 1) was proposed on the basis of low-temperature NMR data.[2] Low-temperature ^{1}H NMR experiments conducted on Rh(allyl)$_3$ also suggested a C_s (C_s-a) structure.[10] For Ir(allyl)$_3$, a ground state structure has yet to be proposed, although solution NMR data indicate two distinct allyl environments at room temperature.[2,4b]

Recent advances in DFT calculations make the prediction of ground state structure and dynamic behavior of organometallic complexes more reliable than in the past.[11] Here we apply hybrid and gradient-corrected DFT methods to Rh(allyl)$_3$ and Ir(allyl)$_3$ to probe the ground state geometry, electronic structure, and molecular dynamics. The remarkable structure and dynamics predicted by these calculations have been verified by variable-temperature NMR, PES, and FT-Raman spectroscopy.

Experimental Section

All manipulations were performed under inert atmosphere or vacuum using standard glovebox, vacuum-line, and Schlenk techniques. Rh(allyl)$_3$ and Ir(allyl)$_3$ were prepared according to the literature method.[2,4] All NMR solvents were degassed and stored over activated 4 Å molecular sieves.

FT-Raman Spectroscopy. FT-Raman spectra of crystalline solids in capillary tubes were recorded at room temperature using a Nicolet Magna-IR 560 spectrometer equipped with a Raman accessory (1064 nm excitation) at 4 cm^{-1} resolution.

NMR Experiments and Data Processing. All NMR experiments were performed on a Bruker DRX 500 instrument equipped with a variable-temperature control. The spectra were collected between −90 and +90 °C on 15 mg samples dissolved in toluene-d_8. The temperature was calibrated using a standard sample of 4% methanol in methanol-d_4. All spectra were processed using XWINNMR 2.6 software (Bruker) with 0.1 Hz line broadening. Resonance line widths were obtained using the deconvolution routine in XWINNMR software. Line widths of solvent resonances were used as an internal standard to correct for possible differences in field homogeneity. The line widths were plotted as a function of temperature, and the limiting line widths were estimated from the plots. The limiting line width and separation of resonances were used to estimate the exchange rates. In the limit of slow exchange, the rates were calculated using the approximation in eq 1.[12] In the fast exchange regime above the coalescence temperature, the rates were calculated using the equation derived by Piette and Anderson (eq 2),[13] where $\delta\nu$ is the separation of resonances in the absence of exchange and T_{2A} and T_{2B} are their respective transverse relaxation times obtained from limiting line widths as $T_2 = (\pi \times \text{limiting line width})^{-1}$.

$$k = (\text{observed line width} - \text{limiting line width}) \times \pi \quad (1)$$

$$k = 0.5\pi(\delta\nu)^2[\text{observed line width} - (T_{2A} + T_{2B})/(2\pi T_{2A}T_{2B})]^{-1} \quad (2)$$

In an Eyring plot (see Supporting Information), the rate data were fitted linearly using the program Origin 4.1 (Microcal) to obtain values of activation enthalpy and entropy for all signals observed.

Photoelectron Spectroscopy. He I and He II gas phase photoelectron spectra of M(allyl)$_3$ (M = Rh, Ir) were measured using a PES Laboratories 0078 spectrometer interfaced with an Atari microprocessor. Spectra were calibrated with He, Xe, and N_2. The samples were held at ca. 40 °C during data acquisition.

Computational

The hybrid B3LYP DFT approximation (as implemented in the G98 package[14]) was used to determine the geometries and associated frequencies of the local minima and transition states connecting them. The metal centers were described by the "small core" LANL2 relativistic core potential[15] and the associated (completely uncontracted) double-ζ basis set augmented with an f-type polarization function ($\alpha = 0.6$). This polarization function was optimized for an organometallic Re complex in earlier B3LYP DFT studies.[16] No attempt was made to reoptimize in the current studies, but we expect the polarization function to be adequate for Rh and Ir. The 6-31G* basis set was used on the ligand atoms. All stationary points were verified to be minima or saddles by explicit computation of the second derivatives of the energy with respect to nuclear displacement. Unless stated otherwise, all energies reported are the sum of the electronic energy and zero-point contribution.

(7) We have collected data on several Rh(allyl)$_3$ and Ir(allyl)$_3$ crystals in addition to samples cocrystalized with triphenylphosphine oxide. All of the data refinements pursued thus far have been handicapped by severe disorder of the allyl framework.

(8) Green, J. C.; Seddon, E. A. *J. Organomet. Chem.* **1980**, *198*, C61. (b) Berry, M.; Garner, C. D.; Hillier, I. H.; MacDowell, A. A. *Inorg. Chem.* **1980**, *20*, 1962.

(9) Swang, O.; Blom, R. *J. Organomet. Chem.* **1998**, *561*, 29.

(10) Becconsall, J. K.; O'Brien, S. *Chem. Commun.* **1966**, 720.

(11) Koch, W.; Holthausen, M. C. *A Chemist's Guide to Density Functional Theory*; Wiley-VCH: New York, 2000.

(12) Sandstrom, J. *Dynamic NMR*; Academic Press: New York, 1982.

(13) Piette, L. H.; Anderson, W. A. *J. Chem. Phys.* **1959**, *30*, 899.

(14) Frisch, M. J.; Trucks, G. W.; Schlegel, H. B.; Scuseria, G. E.; Robb, M. A.; Cheeseman, J. R.; Zakrzewski, V. G.; Montgomery, J. A. Jr.; Stratmann R. E.; Burant, J. C.; Dapprich, S.; Millam, J. M.; Daniels, A. D.; Kudin, K. N.; Strain, M. C.; Farkas, O.; Tomasi, J.; Barone, V.; Cossi, M., Cammi, R.; Mennucci, B.; Pomelli, C.; Adamo, C.; Clifford, S.; Ochterski, J.; Petersson, G. A.; Ayala, P. Y.; Cui, Q.; Morokuma, K.; Malick, D. K.; Rabuck, A. D.; Raghavachari, K.; Foresman, J. B.; Cioslowski, J.; Ortiz, J. V.; Stefanov, B. B.; Liu, G.; Liashenko, A.; Piskorz, P.; Komaromi, I.; Gomperts, R.; Martin, R. L.; Fox, D. J.; Keith, T.; AlLaham, M. A.; Peng, C. Y.; Nanayakkara, A.; Gonzalez, C.; Challacombe, M.; Gill, P. M. W.; Johnson, B.; Chen., W.; Wong, M. W.; Andres, J. L.; Gonzalez, C.; Head-Gordon, M.; Replogle, E. S.; Pople, J. A. *Gaussian 98*, Revision A7; Gaussian, Inc.: Pittsburgh, PA, 1998.

(15) Hay, P. J.; Wadt, W. R. *J. Chem. Phys.* **1985**, *82*, 299.

(16) Pietsch, M. A.; Russo, T. V.; Murphy, R. B.; Martin, R. L.; Rappe, A. K. *Organometallics* **1998**, *17*, 2716.

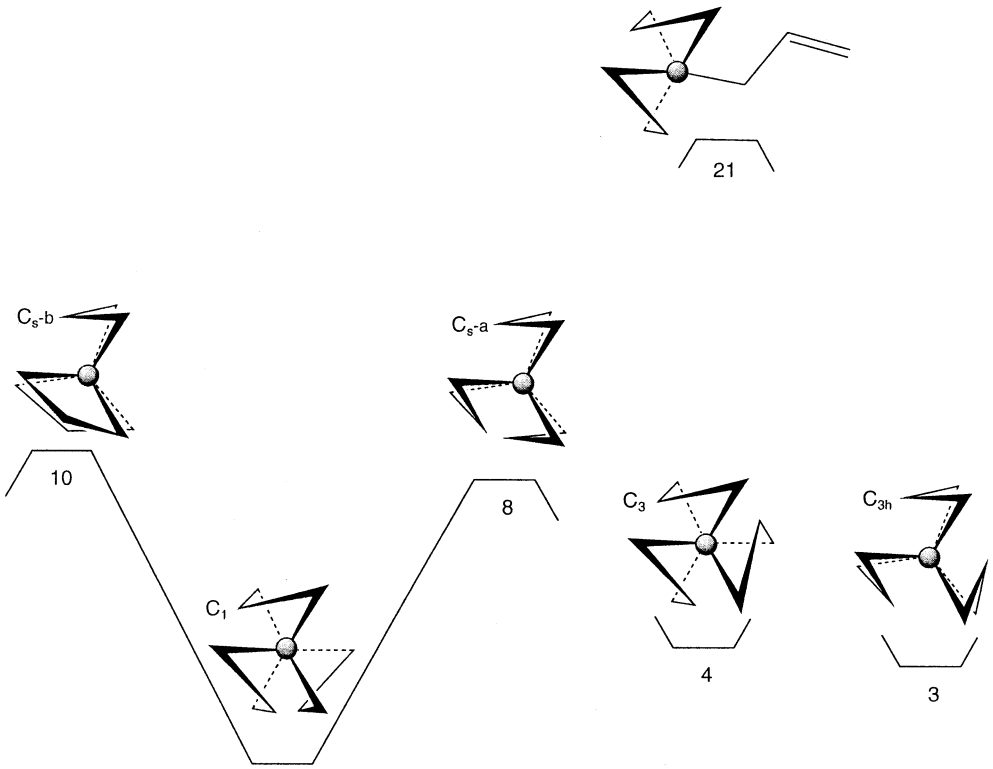

Figure 2. Calculated potential energy surface of $Ir(allyl)_3$ using hybrid DFT (B3LYP). The energies of the states include a zero-point correction (energies in kcal/mol). A similar surface is obtained for $Rh(allyl)_3$; the energies of the transition states C_s-a and C_s-b are 7 and 12 kcal/mol, respectively.

The photoemission calculations were performed at the geometries determined in the B3LYP calculations. They utilized the Amsterdam Density Functional package (Version ADF99).[17] The basis set consisted of triple-ζ accuracy sets of Slater-type orbitals with relativistic corrections and a single polarization function added to the main group atoms. The cores of the atoms were frozen [C (1s), Rh (3d), Ir (4d)]. A gradient-corrected functional (BP86) was applied using Vosko, Wilk, and Nusair's local exchange correlation[18] with nonlocal exchange corrections by Becke[19] and nonlocal correlation corrections by Perdew.[20] Vertical ionization energies were estimated from the difference between the total energy for the molecule and the molecular ion in the appropriate state. Convergence was most readily achieved for the ion states when the initial guess for the SCF calculation utilized the MOs of the molecular calculation. This also enabled a ready check on how precisely the ionic state could be described as a single "hole" in the appropriate MO. Fragment analyses were carried out on $Ir(allyl)_3$ and involved single-point calculations using the MOs of the M and allyl fragments as the basis set for the molecular calculations. The fragments retain the geometries found for the optimized molecular structure.

Results

B3LYP Minima and Transition States. The lowest energy structures found in the B3LYP approximation for both $Ir(allyl)_3$ and $Rh(allyl)_3$ have no symmetry (C_1). The potential energy surface for $Ir(allyl)_3$ is depicted schematically in Figure 2. Note that the skeleton framework is roughly planar; that is, the three methine carbons and the metal center are approximately coplanar. There is slight pyramidalization about the metal site in both species on the order of ∼5 degrees. Using the center of mass of each allyl group and the metal site to determine the plane, the framework group is significantly more planar. Interestingly, the skeleton does not possess a 3-fold rotation axis perpendicular to the plane. Instead, the three methine carbons define an acute triangle. Two of the allyls form a base, while the apical allyl is distinct. In the $Ir(allyl)_3$ case, the Ir−C distances to the two methine carbons forming the base in Figure 2 are identical (2.15 Å), while that to the apical allyl is longer (2.20 Å). This distortion from a D_{3h} framework is similar for $Rh(allyl)_3$ (two Rh−C bond distances at 2.17 Å and one at 2.20 Å). Selected geometric parameters are summarized in Table 1.

Considering now the entire structure, we note that while the ground state possesses no symmetry, it can be related to a more symmetric C_s structure (Figure 2) if each allyl is rotated slightly about the axis connecting the respective methine carbon to the metal. This motion involves a ratcheting of the two basal allyls and a rotation of the apical one (Scheme 1). Two such C_s structures can be generated depending on the sense of rotation of the apical allyl. In one case (C_s-a), the mirror plane contains the three methine carbons defining the skeleton framework. Note that reflection through the mirror plane interchanges the terminal carbons on each basal allyl. In the other structure (C_s-b), the mirror plane is perpendicular to the plane of the skeleton

(17) Baerends, E. J.; Berces, A.; Bo, C.; Boerringter, P. M.; Cavallo, L.; Deng, L.; Dickson, R. M.; Ellis, D. E.; Fan, L.; Fischer, T. H.; Fonseca Guerra, C.; van Gisbergen, S. J.; Groeneveld, J. A.; Gritsenko, O. V.; Harris, F. E.; van den Hoek, P.; Jacobsen, H.; van Kessel, G.; Kootstra, F.; van Lenthe, E.; Osinga, V. P.; Philipsen, P. H. T.; Post, D.; Pye, C. C.; Ravenek, W.; Ros, P.; Schipper, P. R. T.; Schreckenbach, G.; Snijiders, J. G.; Sola, M.; Swerhone, D.; te Velde, G.; Vernooijis, P.; Versluis, L.; Visser, O.; van Wezenbeek, E.; Wiesenekker, G.; Wolff, S. K.; Woo, T. K.; Ziegler, T. *ADF Program System Release 1999*; 1999.02 5.
(18) Vosko, S. H.; Wilk, L.; Nusair, M. *Can. J. Phys.* **1980**, *58*, 1200.
(19) Becke, A. D. *Phys. Rev.* **1988**, *A38*, 2398.
(20) (a) Perdew, J. P. *Phys. Rev. B* **1986**, *33*, 8822. (b) Perdew, J. P. *Phys. Rev. B* **1986**, *34*, 7046.

Scheme 1

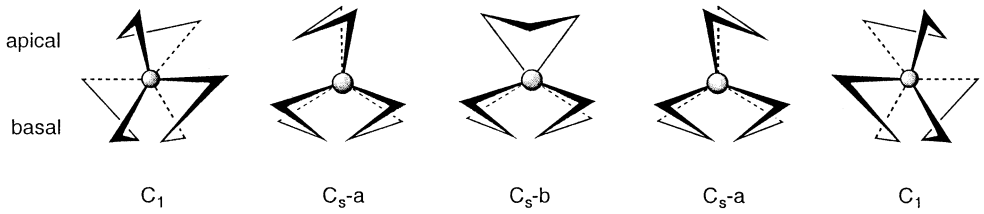

Table 1. Selected Geometric and Energetic Parameters Derived for M(allyl)$_3$, M = Rh, Ir

	C_1	C_s-^{a}	C_s-^{b}	σ-allyl	C_{3h}
Rh(allyl)$_3$					
R_1 (Å)[a]	2.20	2.15	2.15	2.10[d]	2.20
$R_2 \cong R_3$ (Å)[a]	2.17	2.22	2.19	(2.09,2.14)[d] (2.15,2.22)	2.20
E (kcal)	0.0[b]	7.61	12.19	20.37	3.40
ZPE (kcal)	134.0	133.3	134.0	132.5	133.6
S (eu)	104.0	101.6	99.2	108.2	107.2
$\hbar\omega_{imag}$ (cm^{-1})	97	114	136		
Ir(allyl)$_3$					
R_1 (Å)	2.20	2.13	2.11	2.13[d]	2.15
$R_2 \cong R_3$ (Å)	2.15	2.20	2.20	(2.14,2.18)[d] (2.09,2.13)	2.15
E (kcal)	0.0[c]	9.19	9.76	22.74	3.69
ZPE (kcal)	135.1	134.4	135.1	133.2	134.6
S (eu)	102.1	99.7	97.5	109.3	103.5
$\hbar\omega_{imag}$ (cm^{-1})	101	104	99.8		

[a] R_1 is defined as the distance from the apical methine carbon atom to the metal center. $R_2 \cong R_3$ represents the bond distance(s) from the basal methine carbon to the metal center. [b] E = −461.426373 au. [c] E = −456.670859 au. [d] The σ-allyl transition state contains a unique η^1 allyl (here R_1 equals the metal−carbon single bond distance to the σ-allyl group) and two appoximately η^2 allyls (R_2 and R_3 now represent the bound methylene and methine carbon bond distances).

framework. It interchanges one of the basal allyl groups with the other.

Geometry optimizations performed for both of these higher symmetry structures found stationary points, which were determined to be transition states through explicit calculation of the second derivatives. As expected, the reaction coordinate involves the concerted motion of all three allyls. In the case of Ir(allyl)$_3$, both C_s transition states lie about 10 kcal/mol above the ground state.[21] For Rh(allyl)$_3$ the barriers differ significantly, one (C_s-a) being 7 and the other 12 kcal/mol above the ground state.[29]

Note that motion involving passage over the barriers discussed above will make the two basal allyls appear equivalent in ^{13}C NMR at high temperatures (vide infra), but not interchange the basal and apical allyl groups, consistent with the observations of room-temperature NMR reported earlier.[2,10] However, for Rh(allyl)$_3$ we found experimental evidence for exchange of basal and apical allyls at elevated temperatures (vide infra). Stimulated by this observation, we also investigated theoretically a highly symmetric C_{3h} structure. Stationary points were found for both Ir(allyl)$_3$ and Rh(allyl)$_3$. The C_{3h} form lies ∼3 kcal/mol higher in energy than the C_1 structure for both species.[22] We also searched for the C_3 structure depicted in Figure 1. It lies 4.3 kcal/mol higher in energy than the C_1 minimum in Ir(allyl)$_3$ and 3.3 kcal/mol above the minimum for the Rh case.

(21) The magnitudes of the imaginary frequency at the transition state are 104 (114) cm^{-1} for C_s-a and 101 (97) cm^{-1} for C_s-b for the Ir (Rh) complexes.

A final set of calculations was undertaken in order to determine if a simple pathway was available to connect the C_1 structure with the more symmetric C_{3h} one. The C_3 geometry was not considered due to the fact that this geometry is not consistent with high-temperature NMR data (vide infra). While no obvious tris(η^3-allyl) transition states were found, we did locate a σ-allyl species (Figure 3) about 19 kcal/mol above the ground state for Rh and about 21 kcal/mol above the ground state for Ir. These transition states (we were unable to locate a true intermediate) involve an η^3 to η^1 rearrangement of one of the *basal* allyls; subsequent rotation about this single bond will take one to the symmetric C_{3h} structure (Figure 3).[23] This is somewhat of an oversimplification: the two "spectator" allyls also modify their bonding with the metal, rearranging to an unsymmetric bonding mode approaching η^2 in the transition state (Table 1).[24] A final word of caution regarding this transition state is in order. While the transition state appears to be a plausible pathway to connect the two minima, we were unable to follow the intrinsic reaction coordinate from this point in order to verify that it is the lowest path connecting the two.

To summarize the calculations, we find the lowest energy geometry contains three distinct allyls with overall C_1 symmetry. Two of these allyls become equivalent via low-lying transition states of C_s symmetry. The C_1 global minimum is only slightly lower in energy than symmetrical C_{3h} and C_3 structure. A relatively high-energy σ-allyl transition state may connect the C_1 and C_{3h} structures.

FT-Raman Spectroscopy. The Raman data for both Rh(allyl)$_3$ and Ir(allyl)$_3$ have been previously reported.[25] However, spectra were recorded for frequencies at ca. 320 cm^{-1} and above. We were particularly interested in low-frequency data for Ir(allyl)$_3$ since the calculated spectra for the three local minima of C_1, C_3, and C_{3h} symmetry were dramatically different in this region. The most apparent difference in the calculated Raman data is the fact that the C_1 geometry provides many more bands, particularly in the Ir-allyl tilting region

(22) The Ir(allyl)$_3$ case has a perfect C_{3h} local minimum. In the case of Rh(allyl)$_3$, the perfect C_{3h} structure is actually found to be a transition state lying some 1.6 kcal/mol above the local minimum which possesses a pseudo-C_{3h} structure. This minimum (3.0 kcal/mol above the C_1 structure) has three equivalent distances to the methine carbons (2.20 Å), as reported in Table 1, but each allyl has adjusted slightly so as to assume more of an η^2 coordination with the metal. Each allyl is characterized by a trio of distances (2.22, 2.20, 2.29 Å) reflecting the methylene, methine, and methylene metal−carbon distances, respectively.

(23) For an excellent discussion of $\sigma-\pi$ interconversions in allyl complexes, see: Krieger, J. K.; Deutch, J. M.; Whitesides, G. M. *Inorg. Chem.* **1973**, *12*, 1535.

(24) For Ir(allyl)$_3$, the average "η^2" M−C bond distances are 2.12, 2.16, and 2.25 Å, while those of the Rh analogue are 2.12, 2.18, and 2.30 Å.

(25) Andrews, D. C.; Davidson, G. *J. Organomet. Chem.* **1973**, *55*, 383.

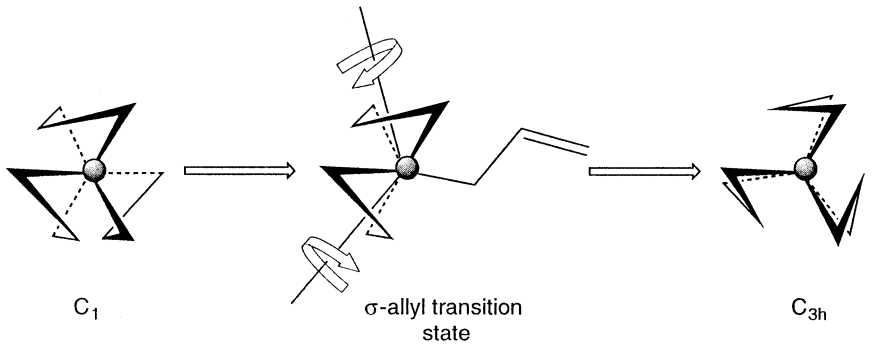

Figure 3. C_1 and C_{3h} structures related by a σ-allyl transition state. The dominant motion in the reaction coordinate is the "flipping" of the σ-allyl group. This occurs through an inversion of the methine carbon in the σ-allyl.

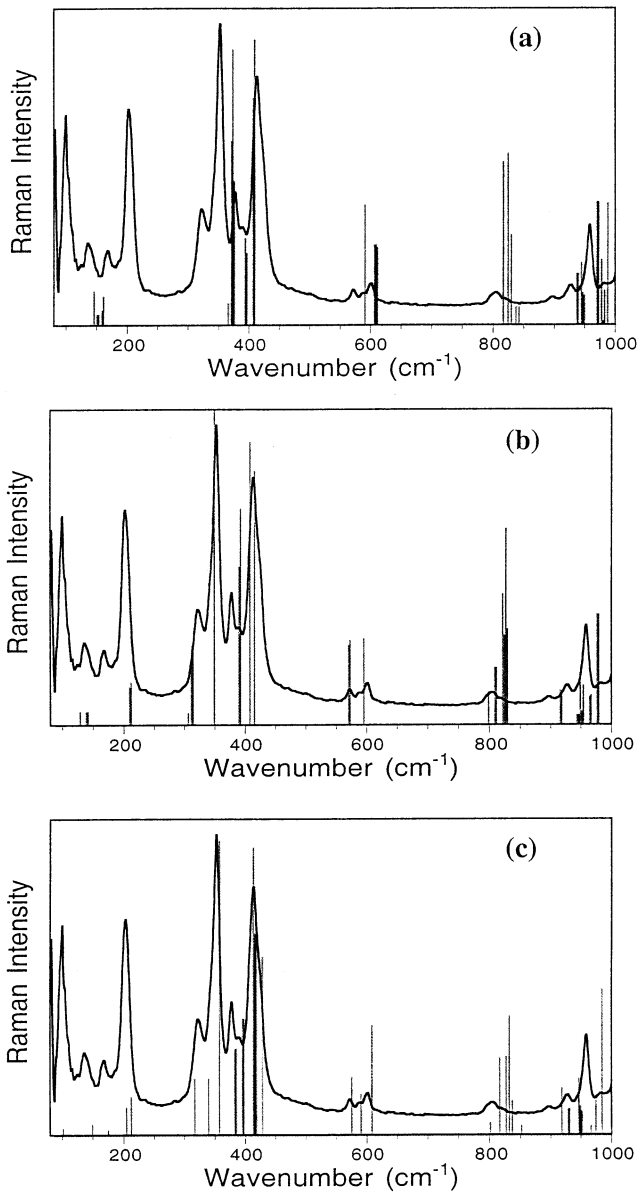

Figure 4. Room-temperature FT-Raman spectrum (1064 nm excitation) of polycrystalline $Ir(allyl)_3$ and predicted spectra (shown as bars) for (a) C_{3h}, (b) C_3, and (c) C_1 minima.

(400−500 cm^{-1}) as well as the allyl torsion region (100−200 cm^{-1}). Shown in Figure 4 is the FT-Raman spectrum of $Ir(allyl)_3$ as a polycrystalline solid at room temperature as well as the calculated frequencies for the C_1, C_3, and C_{3h} geometries. It is apparent that the C_{3h} and C_3 geometries fail to accurately predict the ground state frequencies and intensities below 200 cm^{-1}. In contrast, the C_1 model faithfully reproduces the mode frequencies and intensities in this region and verifies the ground state is of C_1 rather than C_{3h} or C_3 symmetry (the agreement in the 300−400 cm^{-1} range is also much better accounted for by the C_1 structure). Any discrepancies in the intensity for $\Delta\nu < 150$ cm^{-1} are due to the application of a large background correction (KBr) in this region. The excellent agreement between theory and the absolute frequencies for the C_1 geometry is not observed in the higher frequency modes. We begin to observe significant frequency deviations from experiment above 800 cm^{-1} with up to 7% overestimation of the frequencies in the CH stretching region (ca. 3000 cm^{-1}). Such overestimates by 5−10%, particularly in stretching modes, are not uncommon with DFT techniques.

Variable-Temperature NMR. To further confirm that the ground state structure of $Ir(allyl)_3$ is of C_1 symmetry, we have conducted a series of variable-temperature NMR experiments. We will focus on the simpler ^{13}C data since the corresponding ^1H data contain multiple $^1H-^1H$ couplings that complicate the analysis and associated discussion. Low-temperature NMR studies were conducted on $Ir(allyl)_3$ in the range of −15 to −90 °C (Figure 5). Decoalescence of the two symmetry-related methine carbon signals (76 ppm) occurs at roughly −70 °C. At −90 °C, eight distinct allyl signals are observed (two accidentally overlap at ca. 23 ppm) consistent with a C_1 symmetry ground state (a spectrum for the C_{3h} symmetry local minimum would yield only two signals associated with the methine and methylene carbon atoms).[26] Line shape analysis of the methine region provides an activation free energy $\Delta G^{\ddagger}$ of 9.9 ± 1.4 kcal/mol. This value is in reasonable agreement with the value of approximately 8−10 kcal/mol for the activation enthalpy predicted for the C_s symmetry transition states using hybrid DFT methods (vide supra). Low-temperature NMR studies were conducted on $Rh(allyl)_3$ in the range of −10 to −70 °C (Figure 6). At −10 °C we observe two allyl environments due to free rotation of the apical allyl as observed for Ir. Unlike $Ir(allyl)_3$, the energy difference between the C_s-a and C_s-b transition states (ca. 4.5 kcal/mol) manifests itself in the case of the $Rh(allyl)_3$ species. As the sample is cooled to −53 °C, a spectrum consistent with

(26) The low-temperature ^1H data also support a C_1 geometry for $Ir(allyl)_3$. Fifteen separate signals are observed; however, many of them overlap, making line shape analysis difficult.

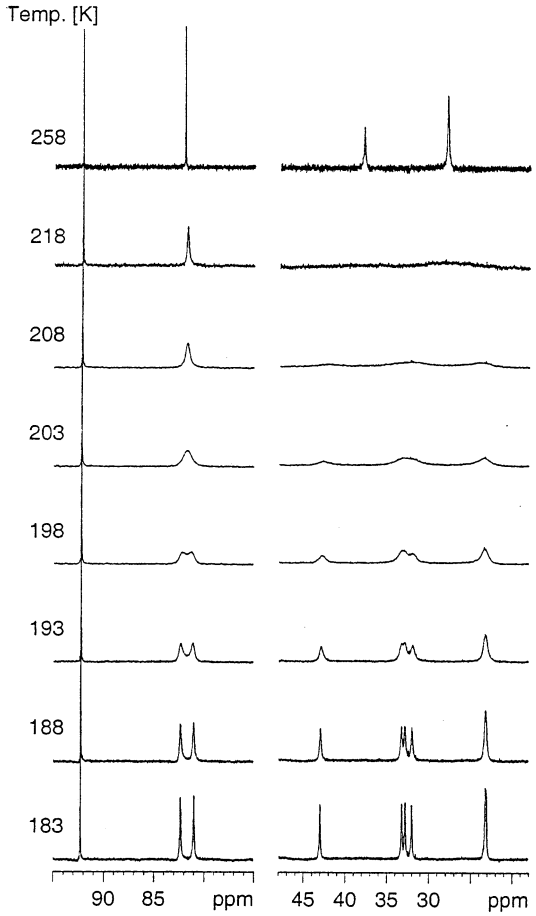

Figure 5. $^{13}C\{^1H\}$ NMR spectra of Ir(allyl)$_3$ between −15 and −90 °C.

a fluxional process involving C_s-a (Figure 6) is observed (equivalent terminal carbons of inequivalent basal allyls), in agreement with the ^1H NMR data obtained by Becconsall and O'Brien.[10] Below −70 °C, further broadening of the terminal carbon resonances is observed, suggesting the complex with C_1 symmetry is accessible at even lower temperatures. Attempts to freeze out the spectrum of the C_1 symmetry complex failed due to crystallization of the sample in toluene-d_8 or precipitation of the complex from other solvents (e.g., pentane-d_{12} or ethanol-d_6). Line shape analysis and fits of the data to the Eyring equation give the activation enthalpy for this transition as 12.9 ± 0.9 kcal/mol (ranging between 12.2 and 14.0 kcal/mol) and the activation entropy as 6.5 ± 2.9 eu (ranging between 4.1 and 10.5 eu). These values determine an activation free energy for the C_s-a transition state of 11.0 ± 1.7 kcal/mol. Note that while the calculated activation enthalpy (12 kcal/mol) is in good agreement with experiment, the theoretical activation entropy has the opposite sign and is −5 eu for C_s-a and C_s-b, respectively.To investigate whether the C_1 and C_{3h} minima are related by a σ-allyl intermediate, high-temperature ^{13}C NMR data for Rh(allyl)$_3$ were recorded in the temperature range 7−73 °C and are shown in Figure 7. The simultaneous broadening of all four ^{13}C NMR signals suggests that a C_3 symmetric structure does not play a role in this transition (a C_3 structure would average the three methine signals but not all six methylene signals). High-temperature data were not obtained for Ir(allyl)$_3$, as significant decomposition occurred before line broadening was observed. Data obtained at 80 and 90 °C for Rh(allyl)$_3$ had to be rejected since no carbon signals were observed upon approaching the coalescence temperature. The lack of signal observed at higher temperatures was not due to thermal decomposition since the signals returned upon cooling. The line widths were plotted as a function of temperature, and the calculated rates were then used in an Eyring plot (see Supporting Information). The line fit provided the values of activation

Figure 6. $^{13}C\{^1H\}$ NMR spectra of Rh(allyl)$_3$ between −10 and −70 °C.

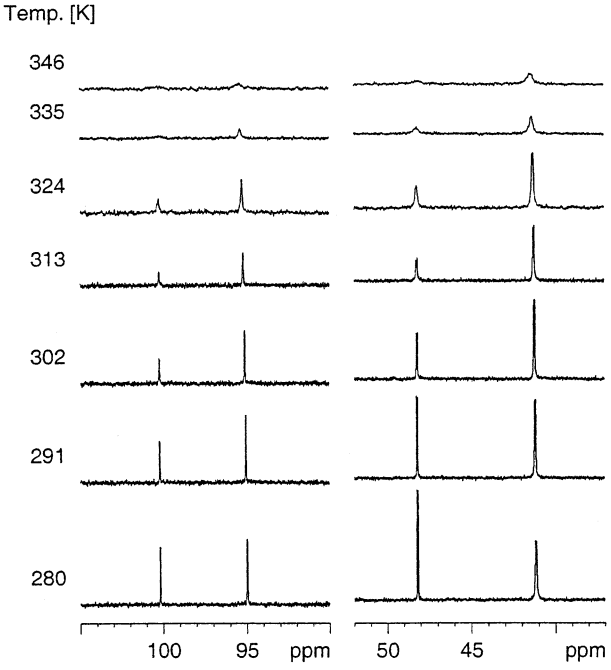

Figure 7. $^{13}C\{^1H\}$ NMR spectra of Rh(allyl)$_3$ between 7 and 73 °C.

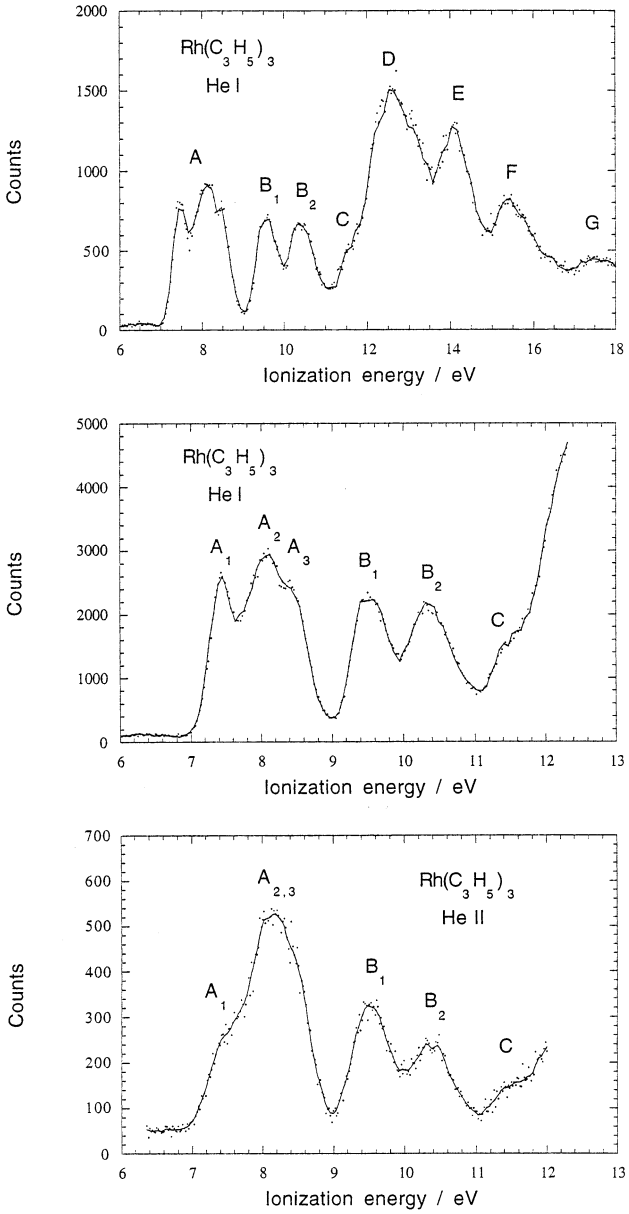

Figure 8. He I and He II photoelectron spectra of $Rh(allyl)_3$.

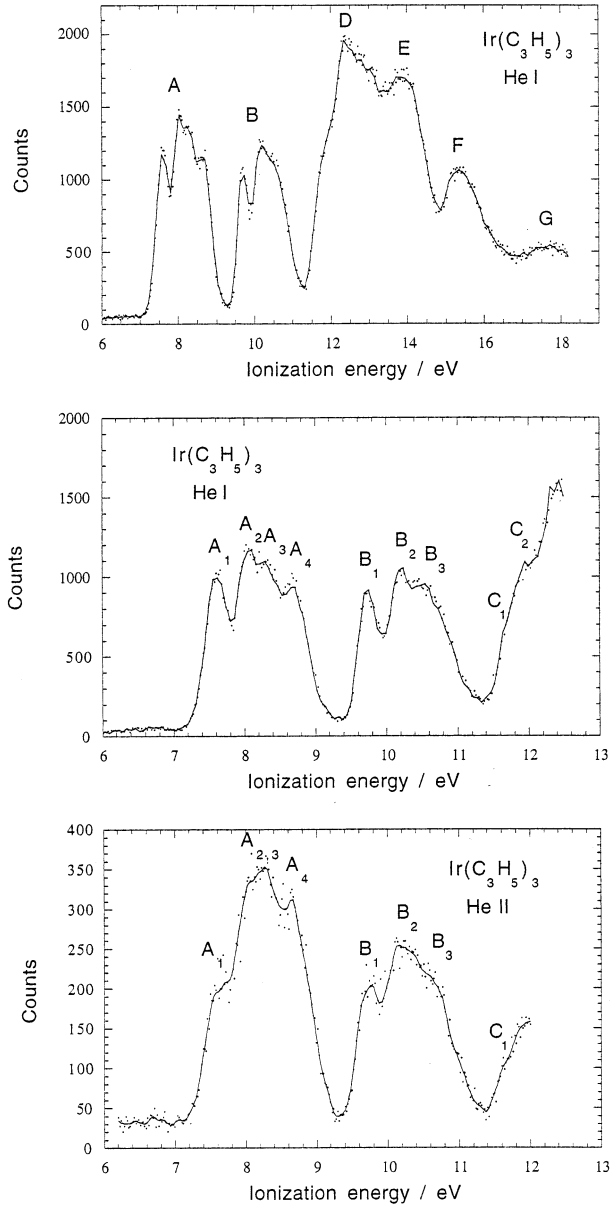

Figure 9. He I and He II photoelectron spectra of $Ir(allyl)_3$.

enthalpy and entropy for all eight signals observed with errors between the values obtained from individual signals. For entropy the values ranged from −7.0 to +17.2 eu, and the values for enthalpy from 14.6 to 22.7 kcal/mol. After rejecting the values deviating from average by more than one standard deviation (two points were rejected), the final results averaged from six values provide an activation entropy of 6.8 ± 2.9 eu and an activation enthalpy of 19.0 ± 1.4 kcal/mol and a resultant activation free energy of 17.0 ± 2 kcal/mol. This value of the activation enthalpy is in excellent agreement with the predicted value of 21 kcal/mol based on the calculated σ-allyl transition state relating the C_1 and C_{3h} minima discussed earlier.

Photoelectron Spectroscopy. The He I and He II spectra of $M(allyl)_3$ (M = Rh, Ir) are shown in Figures 8 and 9, and the vertical ionization energies (IEs) are listed in Table 2. The low-energy bands (IE < 11 eV) fall into two groupings, A and B. The band profiles suggest that there are four ionizations comprising each set of bands. For both $Rh(allyl)_3$ and $Ir(allyl)_3$ the first band, A_1, is clearly separated from the other A bands and appears to decrease in relative intensity in the He II spectrum compared with the other A bands. A_2, A_3, and A_4 all increase in intensity relative to the He II spectra compared with the B bands. In the He I spectrum of $Ir(allyl)_3$, the B bands have a 1 to 3 intensity grouping, whereas for the Rh compound the grouping is 2 to 2. In the $Rh(allyl)_3$ case, B_1 gains intensity relative to B_2 in the He II spectrum. Another difference between the $Rh(allyl)_3$ and $Ir(allyl)_3$ spectra is the shoulder C on the leading edge of the main band. In the spectrum of $Rh(allyl)_3$, the shoulder is readily distinguishable, whereas for $Ir(allyl)_3$ C_1 is barely perceptible on the leading edge of the main band.Oxidation state considerations suggest a $(\pi_1)^6(\pi_2)^6d^6$ configuration for these 18-electron molecules. The PE spectra show a 4:4:1 grouping of the valence ionizations, so spectral assignment is not straightforward in the case of $Ir(allyl)_3$ and $Rh(allyl)_3$ and is aided by computation. DFT calculations of the IE were complicated by the lack of symmetry, so SCF convergence was not achieved for

Table 2. Experimental IE and Calculated Vertical IE (eV) and %d Character of Ground State MO for $M(C_3H_5)_5$, M = Rh, Ir

	Rh exptl		Rh calc	%d	Ir exptl		Ir calc	%d
HOMO	7.42	A_1	7.57	28	7.61	A_1	7.74[b]	46
HOMO-1	8.07	A_2	8.04[b]	62	8.07	A_2	8.18[b]	42
-2			8.18[b]	34	8.28	A_3	8.27	31
-3	8.41	A_3	8.65	64	8.69	A_4	8.75	54
-4	9.51	B_1	9.64[b]	45	9.73	B_1	*a*	13
-5			*a*	28	10.20	B_2	9.92[b]	33
-6	10.32	B_2	9.88[b]	28	10.73	B_3	10.08[b]	17
-7			10.12	12	10.73		10.18	33
-8	11.5	C	10.97	<1	11.6	C_1	11.05	<1
					11.9	C_2		
	12.5	D			12.4	D		
	14.1	E			13.8	E		
	15.4	F			15.3	F		
	17.4	G			17.6	G		

[a] SCF convergence was not achieved for these ion states. [b] Ion states where hole wave function is <85% of the originating ground state MO.

Table 3. Occupancy of Fragment Orbitals in $Ir(C_3H_5)_5$

allyl **1**			allyl **2**			allyl **3**		
π_1	π_2	π_3	π_1	π_2	π_3	π_1	π_2	π_3
1.66	1.13	0.21	1.66	1.11	0.28	1.64	1.15	0.26

Ir 5d					Ir 6s	Ir 6p		
z^2	x^2-y^2	xy	xz	yz		x	y	z
1.75	1.68	1.40	1.45	1.35	1.12	0.22	0.28	0.28

all ion states. Nevertheless, estimates were obtained for the majority of the top nine IE for both compounds; the values are given in Table 2. For both compounds agreement between experiment and theory for the first four ionizations was excellent. For the next five bands there was still good agreement, but the calculations tended to underestimate the IE. The intensity change between He I and He II for a band normally correlates with the d orbital contribution to the MO from which the electron is ionized.[27] The calculated %d content of the orbitals is also given in Table 2. The correlation of relative intensity increases with photon energy, and the d content agrees well for $Rh(allyl)_3$. For $Ir(allyl)_3$, the comparison between bands A_{1-4} and bands B_{1-3} is in line with the higher d content of the former, but band A_1 is anomalous in that it shows a decrease in intensity with respect to the rest of band A, whereas the HOMO has comparable d content. If the nature of the holes in the ion state calculations are examined, several of them are found to differ significantly from the ground state orbital they would be associated with in a one-electron picture of the ionizations. Those with <85% of the parent MO are indicated in Table 2. The ground state for $Ir(allyl)_3^+$ was recalculated using an atomic orbital basis set, and the hole was found to have considerably less d character (13%) and 10% p_z character. Thus it is clear that considerable electronic reorganization takes place on ionization of this molecule.

Discussion

Bonding Model. The lack of symmetry in the ground state structures of $M(allyl)_3$ (M = Rh, Ir) makes a simple description of the bonding in these compounds difficult, as the normal basis set of ligand and metal d orbitals lose their separate identities. Fortunately, there are some helpful indicators from the calculations. The C−C distances in the allyl groups indicate that they retain significant π bonding (Table 1). Fragment analysis of $Ir(allyl)_3$ provides values for their occupancy in the complex shown in Table 3. Principal mixing with the metal orbitals occurs through the π_2 orbitals that are best matched in energy with the metal d orbitals and less so through the π_1 and π_3 orbitals.

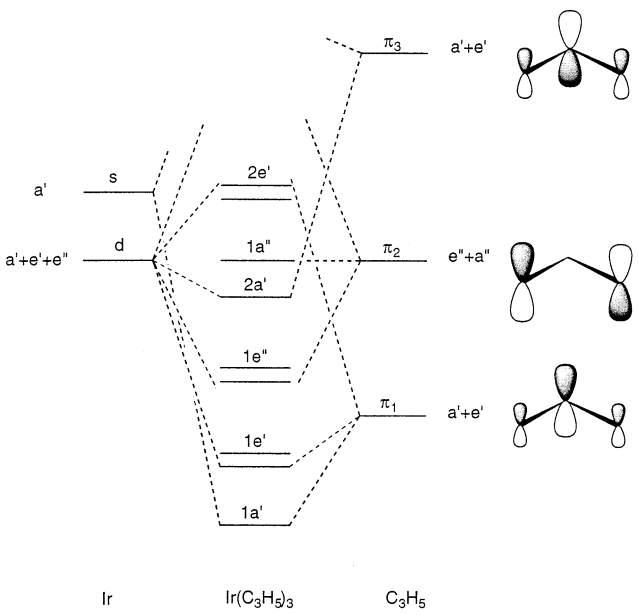

Figure 10. Qualitative orbital scheme for $Ir(allyl)_3$.

It is helpful to consider the bonding in the C_{3h} higher energy structure where the symmetry may be used to define clearly the role of the fragment orbitals. A qualitative orbital scheme is shown in Figure 10. The a′ and e′ combinations of the π_1 orbitals mix with the metal s and d(xy, x^2-y^2), respectively. The π_2 orbitals form an e″ combination, which can bond with the d(xz, yz) orbitals, and an a″ combination, which is effectively nonbonding, the metal p_z contribution being small. The d(z^2) orbital is nodally compatible with the a′ in-phase combination of π_3 orbitals. The 18-electron count ensures that the 2e′ HOMO, which is metal−ligand antibonding, is occupied. Thus, in effect, most metal−ligand bonding results from overlap of the 1e″ orbitals.

For $Ir(allyl)_3$ the C_{3h} structure is calculated to lie 3 kcal/mol above the ground state. The calculated orbital energy levels for the C_1 ground state are correlated with those of the C_{3h} structure in Figure 11. The correlation is based on the d orbital character, but, given the substantial change in symmetry, much mixing between orbital types occurs and the correlation is inevitably somewhat arbitrary. On passing from the symmetric to the unsymmetric structure, the 2e′ orbitals are stabilized and the 1e′ orbitals destabilized, indicating an avoidance of the π_1 d(xy, x^2-y^2) repulsion. Also the three orbitals correlating with the π_2 orbitals, a″ and e″, are significantly stabilized, and the reasons for this may be understood by the nature of the distortion.

In the C_{3h} structure, the centroids of the allyl groups lie on a plane that includes the metal atom with trigonal symmetry about the plane (Figure 12a). If we take this

(27) Green, J. C. *Acc. Chem. Res.* **1994**, *27*, 131.

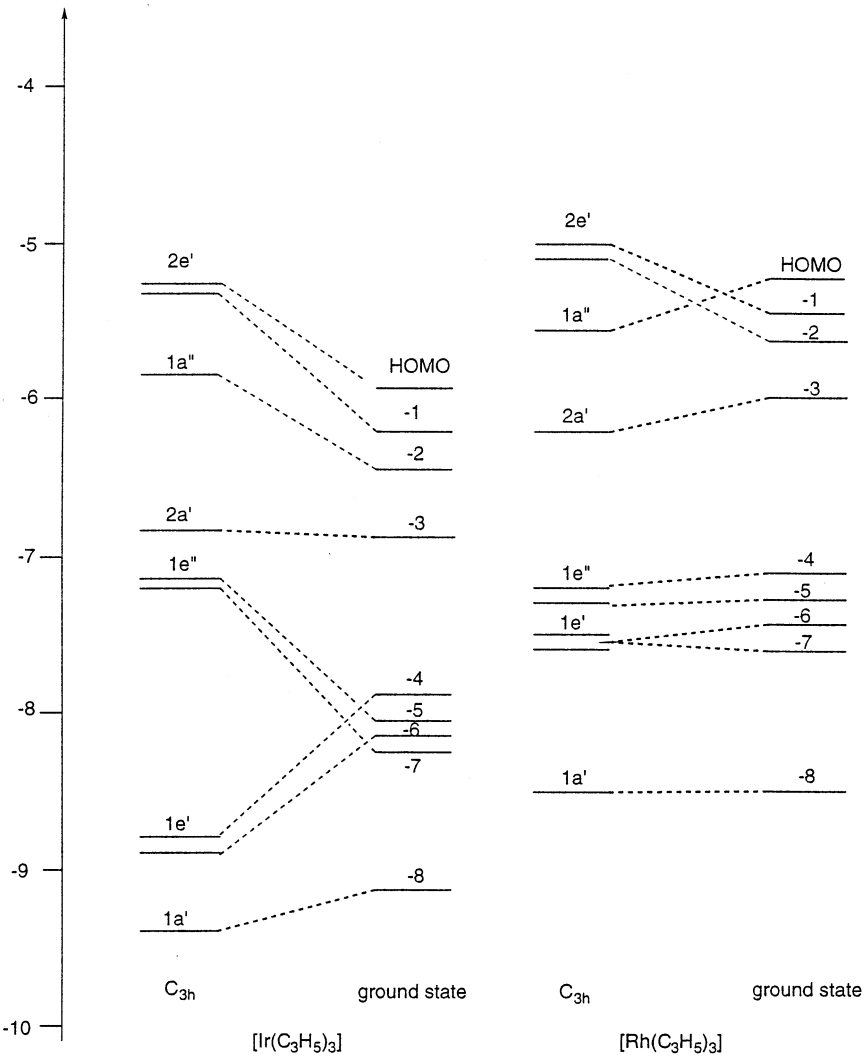

Figure 11. Gradient-corrected DFT-calculated orbital energies for $M(allyl)_3$.

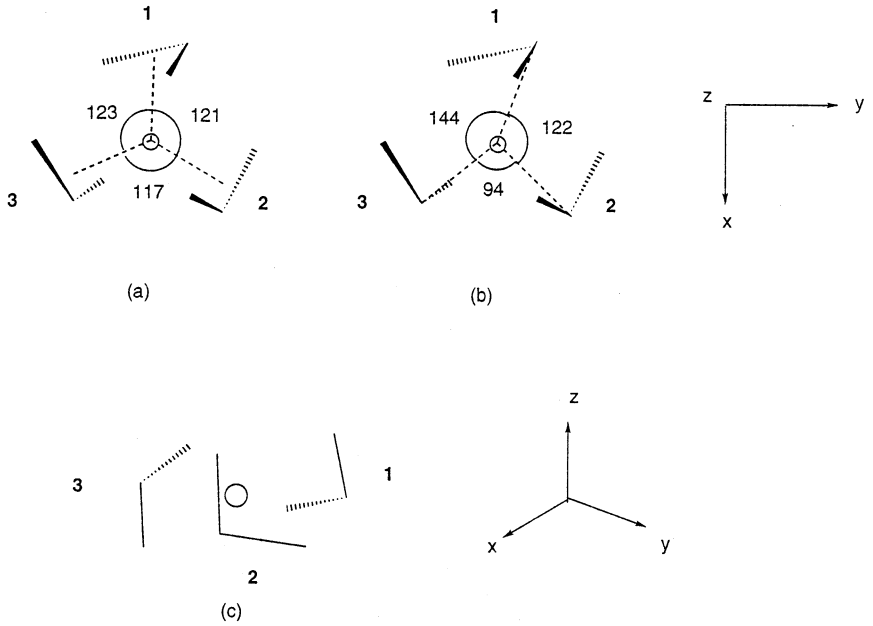

Figure 12. (a) Angles subtended at Ir by centroids of allyl ligands. (b) Angles subtended at Ir by C2's of allyl ligands. (c) Tilt of allyls from Ir centroid plane.

as the *xy* plane of the molecule, the modification from C_{3h} to C_1 symmetry consists of flipping one of the allyl ligands (allyl **3** in Figure 12) and rotating all three so that one of the C−C bonds in each lies roughly perpen-

dicular to the plane (Figure 12c). Thus the terminal carbons move from trigonal prismatic coordination (Figure 12a) toward octahedral coordination (Figure 12b). *As a consequence, all three combinations of π_2 orbitals become bonding.*

The three central allyl carbons lie close to the *xy* plane, but, as a result of the flipping of one of them, they are not trigonally disposed (Figure 12b). Angles subtended by them at the metal are 94°, 122°, and 144°. Presumably their unsymmetrical distribution polarizes the electron density in the *xy* plane toward the most open angle and avoids the nonbonded repulsion inherent in a symmetric trigonal structure. Noteworthy in this context is that the x^2-y^2 orbital has a higher occupancy than the *xy* orbital.

For Rh(allyl)$_3$ the calculated difference in energy between the C_{3h} and the C_1 ground state structures is similar. The orbital correlation for these two structures is also shown in Figure 11. In the Rh(allyl)$_3$ case, the energy changes are more subtle and relief of the antibonding character of the 2e′ orbital appears to be the principal stabilizing force.

Dynamic Behavior. Since the initial characterization of both Ir(allyl)$_3$ and Rh(allyl)$_3$, it has been apparent that the behavior of these compounds in solution at room temperature involves multiple fluxional processes. The ^{1}H NMR data have been explained previously by the apical allyl rapidly rotating relative to the other two allyl groups.[2] With respect to our potential energy surface (Figure 2) discussed earlier, this rotation can be understood in terms of a concerted motion in which the unique allyl group rotates completely about its axis and the other two allyl groups "ratchet" back and forth in a symmetric manner to accommodate this rotation. The complete rotation involves two transition states, C_s-a and C_s-b.

Furthermore, in the case of Rh(allyl)$_3$, we have been able to observe evidence of basal allyl ratcheting *without* free rotation of the apical allyl. We are able to observe this phenomenon due to the ca. 5 kcal/mol energy difference separating the C_s transition states. In addition, we have low-temperature ^{13}C NMR evidence that suggests the existence of a C_1 symmetry ground state for Rh(allyl)$_3$ (unlike the C_s-a ground state proposed previously[10]).

A further surprising result from this study is the lack of a simple mechanism to interconvert the C_1 and C_{3h} structures while maintaining three η^3-allyl ligands. Instead we have identified a σ-allyl transition state that allows for rotation about one of the C−C bonds. This σ-allyl may also serve as a mechanism to explain the observed reactivity of these complexes. It is apparent that the fluxional processes in these molecules require concerted motions of the apical and basal allyls. The prospect of ligand addition without an open coordination site seems quite improbable given this apparent steric congestion.[28] A σ-allyl intermediate may also allow a pathway for associative substitution reactions. For example, we can systematically convert the σ/π manifold of Ir(allyl)$_3$ from Ir(π-allyl)$_2$(σ-allyl)L [L = PPh_3, SCN-Tol] to form Ir(π-allyl)(σ-allyl)$_2$L$_2$ [trans-allyl: L = PMe_3; cis-allyl: L$_2$ = o-dppb] and Ir(σ-allyl)$_3$L$_3$ [L = CO, CNR, triphos] through judicious choice of donor ligands. Studies are currently in progress to determine the implication of a σ-allyl transition state upon the kinetics of formation of the above complexes.

(28) This concept of steric congestion may explain why we have not been able to prepare M(2-Me-allyl)$_3$ or M(allyl)$_2$(2-Me-allyl).

Conclusion

A combination of theoretical and experimental techniques has revealed the remarkable structure and dynamics of Ir(allyl)$_3$ and Rh(allyl)$_3$. The picture that has emerged is consistent with both theory and a diverse set of experimental probes. The preferred ground state structure has no symmetry due to an orbital preference of octahedral C_1 over C_3 or trigonal prismatic C_{3h}. Three distinct fluxional processes have been identified involving ratcheting of the basal allyls, rotation of the apical allyl, and a σ-allyl intermediate. DFT calculations of ionization energies give good agreement with the experimental PE band positions especially for the first four ionizations of both compounds. The ionizations involve considerable reorganization of the MO composition upon ionization. Interpretation of the He I and He II intensity changes takes this into account. The relative stability of the C_{3h} and ground state C_1 structures can be accounted for by the more effective bonding of the π_2 orbitals in the ground state C_1 structure, where the terminal carbons of the allyls are closer to the preferred octahedral coordination, as well as the avoidance of π_1 d nonbonded repulsion in the unsymmetrical structure. While the error bars on computational DFT studies are still fairly large, the combination of theory with experiment yields a powerful synergy in sorting out the molecular geometries and properties of compounds that resist conventional structural characterization techniques. Future studies will focus upon the application of these models to aid in the analysis of the reactivity of these and related complexes. Additional experiments will focus on mechanistic studies aimed at understanding general reactivity trends both in solution and on metal oxide supports.

Acknowledgment. We thank the Department of Energy's Laboratory Directed Research and Development (LDRD) program as well as the Department of Energy, Office of Basic Energy Sciences, Chemical Science Division, for financial support. We thank the referees for their constructive and insightful comments. We would also like to thank Dr. Judith Eglin and Dr. David Thorn for helpful discussions and assistance with the manuscript. Part of this work was carried out using the resources of the Oxford Super-Computing Centre and part using the EPSRC Columbus cluster at the Rutherford laboratory.

Supporting Information Available: Eyring plots associated with M(allyl)$_3$. This material is available free of charge via the Internet at http//pubs.acs.org.

OM020632P

(29) One of the reviewers of the manuscript expressed concern over the possibility of a missing factor of 2 in our calculations because we failed to account for two C_1 symmetry enantiomers. While we do agree that this would be an issue if we were concerned with equilibrium rate constant *s* between chiral and nonchiral species, we feel that this makes no difference to the activation energy/enthalpy, as these are temperature derivatives of the rate constant and any temperature-independent statistical factor would not contribute.